# Deposition and Removal Studies of Asphaltene from Glass Surface

Syed Haider Abbas Rizvi, Anil Yadav, Jyoti Phirani, and Vikram Singh*

*Department of Chemical Engineering, Indian Institute of Technology Delhi, Hauz Khas, New Delhi, India - 110016*

E-mail: vs225@chemical.iitd.ac.in

**Abstract**

Asphaltene deposition in crude oil reservoirs and transportation lines affects the oil recovery and incurs additional operational costs. The current study discusses the removal of asphaltene from inorganic silica surfaces using hydrodynamic forces. The deposition of asphaltene was carried out on clean glass slides (proxy material for silica) from heptane-asphaltene dispersions via aging. For the removal of asphaltene, a parallel plate channel is fabricated with a pocket to place aged substrates under varying shear rates. The apparatus enables studying the surface morphology changes on a glass slide due to controlled flow conditions through physical contact techniques like atomic force microscopy (AFM). The AFM characterizes the extent of both deposition and removal of asphaltene from the surface. The results show that large aggregates of asphaltene are removed from the surface with an increase in flow rates. The extent of removal of asphaltene from the substrate as a function of shear rate is determined. The study also discusses the possible mechanism of asphaltene removal from the surface using the hydrodynamic force calculations. The colloidal interactions calculated from hydrodynamic forces are reported to be $F_{adh}/(d/2) = 1.29$ mN/m. The presence of asphaltene tends to alter surface wettability. Interestingly the contact angle measurements carried



This is a peer-reviewed, accepted author manuscript of the following article: Rizvi, S. H. A., Yadav, A., Phirani, J., & Singh, V. (2021). Deposition and removal studies of asphaltene from the glass surface. Energy and Fuels, 35(4), 3228-3239. https://doi.org/10.1021/acs.energyfuels.0c03881

out on the asphaltene deposited glass slides and after removal of asphaltene from the surface showed a negligible change, indicating incomplete removal of asphaltene from the surface.

# 1 Introduction

Asphaltenes are naturally occurring heavier components which remain soluble in crude oil. However, they phase separate as a result of changes in temperature, pressure, and composition.[1–4] Asphaltenes are defined based on solubility as the component of the crude oil that is insoluble in lower alkanes such as *n*-pentane or *n*-heptane but soluble in polar aromatic solvents like benzene or toluene.[5,6] The polar nature of asphaltenes is due to the presence of naphthenic and aromatic rings in the core and acidic groups at the tails.[7] When asphaltenes phase separate, they remain suspended in the crude oil, forming a colloidal system and can get deposited on the surfaces in contact.[8] The deposition of asphaltenes causes blocking of pores in oil reservoirs, clogging of transportation lines, and fouling of refinery equipment. Therefore, the removal of asphaltene from the surfaces is a significant challenge for the oil and gas sector.[9–12]

In the crude oil industry, various chemicals (solvents, detergents, and polymers), thermal, or mechanical modes are adopted for asphaltene removal.[13,14] However, there is not a broad acceptance for solvent removal and thermal treatments due to toxicity reasons and high operational costs. This study aims to develop an insight into asphaltene removal through mechanical mode using shear forces.

In this work, we deposited the asphaltene on glass used as a proxy substrate for silica. It is well known that a borosilicate glass that has $SiO_2$ content over 80% is widely accepted to mimic properties similar to sand found in the crude oil systems.[15] The asphaltene removal from the surface of the glass slide is in an apparatus where changing the flow rate tunes the shear forces on the surface. The flow inside the apparatus is of the order of Reynolds number from $2.1 \times 10^3$ to $1.4 \times 10^4$. The extent of removal is quantified using the atomic

force microscopy on the substrate.

Several researchers have been conducting experiments over the past few decades to understand the mechanism of asphaltene deposition on the surfaces. The studies suggest that asphaltene aggregate formation and deposition occurs because of the van der Waals, Coulombic, and repulsive exchange interactions[16,17] between asphaltene molecules and asphaltene and surfaces. Natarajan et al.[18] investigated the nature of such asphaltene-asphaltene and asphaltene-substrate interactions. The results suggest the presence of long-range steric repulsion between asphaltene layers and bridging adhesion between asphaltene and hydrophilic surfaces in organic solvents. Force measurements between asphaltene and silica surfaces in toluene and aqueous media have also been carried out by Wang et al.[19] and Abraham et al.,[20] respectively. Wang et al.[19] findings suggest that interactions in toluene, such as steric repulsion, vary with deposition techniques. A more compact or organized film has a higher and more extended range of repulsive forces. Abraham et al.[20] stated that the morphology of films and forces of interaction is a function of salinity and pH of the aqueous media. The swelling/stretching of surface asphaltene is due to molecular rearrangements.

In a similar context, Labrador et al.[21] also conducted studies with toluene-asphaltene solutions of concentrations ranging from 200-10,000 mg/L and reported the thickness of deposited asphaltene films on glass varying in the range of 20-298 nm. In a different study with asphaltene solutions prepared in heptane-toluene mixtures, Soorghali et al.[22] reported the roughness of two distinct substrates characterized by atomic force microscopy to be 168 nm and 56.6 nm, respectively. The authors stated the difference in roughness as a result of different origins of asphaltene. Both of these individual studies[21,22] suggest that asphaltene aging results in a deposition thickness of a few hundred nanometers on glass surfaces, which is also a function of asphaltene concentration.

The precipitation of asphaltenes in the lower alkane systems is higher than toluene-based systems because of polar asphaltene and non-polar solvent interactions.[23] A higher amount of asphaltene phase separates from a pure heptane system compared to the toluene-heptane

system leading to more extensive depositions of asphaltene on all contact surfaces. The effect of aging time, i.e., the period of deposition, also plays an essential role in determining the degree of deposition.[20,24–26] The present study considers a constant aging time of 24 hours for sufficient deposition of asphaltene on the surface.

Mechanical forces, such as the fluid-induced shear forces, have been used in the past to remove colloidal[27,28] and aerosol[29] particles from surfaces. For particle removal, the hydrodynamic forces applied have to overcome the adhesion forces between the particle and the surface.[30,31] Researchers have also used this method for the removal of polymeric materials from metallic surfaces,[32,33] soot particles from exhaust pipes,[34] and for latex and polystyrene microspheres from glass and poly-acrylamide surfaces.[35,36] Meinders et al.[37] also observed adsorption and removal of the colloidal polystyrene particles on glass in a parallel plate channel and found an enhanced removal on increasing the shear rates.

We discussed in brief the background about the work conducted so far. The majority of the studies in the literature have systems in which asphaltene is present in a preferably soluble state with toluene. In this work, we are interested in observing the deposition of asphaltene dispersed in a non-polar pure $n$-alkane system with hydrophilic silica substrates to mimic for higher deposition of asphaltene in reservoirs or pipelines. The next section describes the methodology used in the study for the extraction of asphaltene and preparing substrates. In the same section, we have provided detailed design of the parallel plate channel and experiments to observe the removal of asphaltene from the substrates. The continuing section shows the results of these experiments after the atomic force microscopy. The morphology (height sensor) and phase angles of the asphaltene substrates is related to the amount of asphaltene on the surface. The reduction in surface roughness, in general, corresponds to the relative removal of asphaltene as a function of shear rates. The study also suggests estimates of colloidal interactions (adhesion forces and hydrophobic interactions) based on the hydrodynamic forces implemented for asphaltene removal. The estimation of magnitudes of these forces is through generalized correlations for adhesion and removal

of particles from the surface. The analysis of AFM images provides an approximation of particle size for such calculations. The study also holds substantial industrial significance suggesting removal modes of asphaltene from silica surfaces using shear forces.

# 2 Experimental

A systematic process is adopted to investigate the interaction of asphaltene with surfaces. We have used glass slides as a proxy material for silica present in contact with the crude oil in the reservoirs or pipelines. The clean substrates are aged in dispersions of asphaltene and heptane for surface deposition (Figure 1a) of asphaltene. After aging in the heptane-asphaltene mixture, the slides are rinsed (dipped and removed immediately) in pure heptane to ensure the removal of free asphaltene in the film on the substrates that may cause inconsistency of results (Figure 1b). The substrates to be investigated for deposition only are directly sent to drying for 24 hours and analyzed through atomic force microscopy (Figure 1c). In the other set of experiments, the deposited asphaltene is removed from the surface using hydrodynamic forces in a parallel plate channel. The parallel plate channel has a carved pocket such that any substrate having dimensions that of a glass slide (75 x 25 mm) can be inserted (Figure 1d). The substrates from the parallel plate channel are dried (24 hours) and then sent to the AFM. The extent of deposition/removal is quantified in terms of change in the surface roughness. The presence of asphaltene also alters the wettability of the surface.[3,38,39] The experiments also involve the measurement of the contact angle of a water droplet on the substrate at each step.

## 2.1 Asphaltene Extraction

Asphaltene extraction is done in-situ from 55% bitumen emulsion with kerosene (Shalibond, provided by STP Ltd) via ASTM D2007-80 standard procedure.[40,41] A pre-defined amount of bitumen is added to *n*-heptane (HPLC grade, Fisher Scientific) in the ratio 1:40 (w/v). This

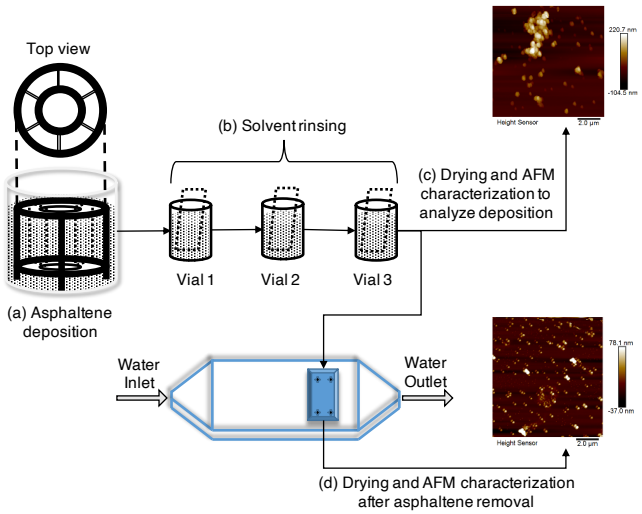


Figure 1: Process diagram: (a) Method for deposition of asphaltene on glass slides: The glass slides are held upright in a stainless steel assembly placed inside a beaker containing asphaltene in a model-oil solution. The beaker is covered to prevent solvent vaporization. The solution is stirred on a magnetic stirrer operating at 450 RPM and 90°C. (b) Rinsing of aged substrates to remove free asphaltene. The glass slides are completely immersed in each vial and removed immediately. (c) Drying of substrates deposited with asphaltene at 90°C for 24 hours, followed by AFM characterization. (d) Removal of asphaltene in a parallel plate channel and AFM characterization after drying the substrates.

mixture is sonicated for 45 minutes and equilibrated for 24 hours, proceeded by filtration on a 0.45 $\mu$m pore size paper (Whatman). The retentate on paper is further washed with recycling heptane (vapor) in a Soxhlet extractor to dissolve the heptane soluble impurities. The content is further diluted in 1000 ml of toluene (HPLC grade, Fisher Scientific) and filtered to remove toluene insoluble components. The vaporization of toluene is carried out in a rotary vacuum evaporator. The left-over black colored solids (asphaltene) are weighed and properly stored away from moisture until further use.

## 2.2 Asphaltene Deposition on the Glass Slides

Before the deposition of asphaltene, the glass slides are pre-cleaned with rinsing in the surfactant solution (Teepol, CDH Fine Chemicals) and DI water to remove dirt, fingerprints, and grease. The procedure for cleaning is as follows. The slides are first rinsed in a surfactant solution and then thoroughly cleaned with DI water. These slides are later sonicated with

isopropanol (Fisher Scientific) and DI water again for 10 minutes in each. The clean glass slides are dried with nitrogen and later used for the deposition of asphaltene on the surface.

A schematic diagram of the setup used for asphaltene deposition on the glass slides is shown in Figure 1a. The glass slides are held vertically inside a beaker containing the aging mixture for deposition on the glass surfaces. A cylindrical stainless steel holder with annular spacing is used to support six glass slides at a time. The top view of Figure 1a shows the slide holder carrying the glass slides. The aging mixtures are dispersions prepared in $n$-heptane with an asphaltene concentration of 0.03 g/L (constant for all the experiments). The steel holder, along with the glass slides, is immersed in the beaker containing the aging mixture. The cling film firmly wraps over the beaker mouth to prevent solvent vaporization. The aging (deposition) is carried out at 90°C under continuous stirring at 450 RPM for 24 hours.

The asphaltene concentration is chosen based on no visibility of precipitates at the bottom of the beaker after four hours of mixing at 90°C. In the absence of stirring during deposition at 90°C, asphaltenes settle at the bottom of the beaker with the heptane solution being nearly transparent. This suggest that the aggregate sizes are at least to the tune of at least a few hundred nanometers and larger in the suspension. With stirring, but at lower temperatures, asphaltene aggregates tend to settle in the dead zones of stirring assembly. We agree that the temperature of 90°C may slightly affect the dynamics of adsorption/deposition, though it is suited for the study. The downhole temperatures can rise to around 180°C,[42] which reduces to 50-70°C during drilling processes.[43]

## 2.3 Setup for Asphaltene Removal

A parallel plate channel fabricated from stainless steel (SS316 grade) is used to study the removal of asphaltene from the glass surfaces. The channel has a pocket to place a glass slide. The pocket has a cap, tightened through screws to prevent leakage during the flow experiments. The slide rests at the height of four mm from the bottom plate and 300 mm from the inlet where the fully developed flow is assumed. Figure 2 shows the top view and

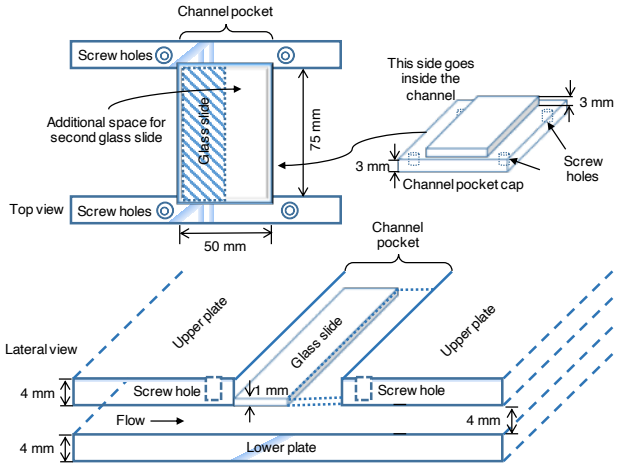


Figure 2: Top view and lateral view of a section of the parallel plate channel. The schematic mentions the dimensions of the channel. At the channel pocket, two glass slides are placed adjacent to each other. That pocket has a cap, tightened through screws to prevent leakage during flow experiments.

lateral view of a section of the parallel plate channel, highlighting the pocket for substrate placement. The pocket can hold two microscopic glass slides adjacent to each other. In our experiments, the asphaltene aged substrate is at the first slot in the direction of flow. A clean glass slide occupies the other slot.

The parallel plate channel operates as a continuous system, as shown in Figure 3. For each run, the setup operates for 20 minutes, where DI water is pumped across the channel by a centrifugal pump. The steel cooling jacket reservoir maintains the temperature of the circulating water at the ambient value. A gate valve controls the flow rate, and a rotameter records it. The corresponding shear rates on the glass slide surface are calculated by simulations on ANSYS Fluent using the $\kappa - \epsilon$ model. The turbulent model simulates the high Reynolds number ($Re$) flow conditions used in the experiments for the removal of asphaltene.[1] Table 1 shows the obtained shear rates from the simulations performed.

[1]The Reynolds number is defined as, $Re = \frac{4hv_{avg}\rho}{\mu}$, where, $4h$ is twice the separation between the plates, $v_{avg}$ is the average velocity at the cross-section where the substrate is placed, $\rho$ and $\mu$ are density and viscosity of water, respectively.

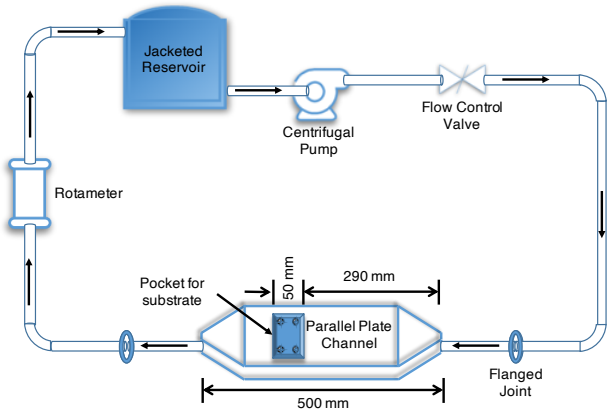


Figure 3: Schematic of flow assembly. Water can be pumped from the reservoir across the parallel plate channel where substrates can be placed. The desired flow rate is maintained through pump and valves, and a rotameter records the value.

Table 1: Shear rates close to the glass slide surface inside the parallel plate channel obtained from ANSYS Fluent simulations using the $\kappa - \epsilon$ model.

| **Flow Rate** $dm^3.h^{-1}$ | **Reynolds Number** $[-]$ | **Shear Rate** $(\dot{\gamma})$ $s^{-1}$ |
|---|---|---|
| 250 | $2.08\times10^3$ | $1.23\times10^3$ |
| 450 | $3.75\times10^3$ | $3.03\times10^3$ |
| 850 | $7.08\times10^3$ | $5.46\times10^3$ |
| 1250 | $1.04\times10^4$ | $1.69\times10^4$ |
| 1650 | $1.37\times10^4$ | $2.37\times10^4$ |

## 2.4 Characterisation through Atomic Force Microscopy (AFM)

In this study, the AFM analyzes the glass slide's surfaces after the completion of the flow experiments. The atomic force microscope (Model Bruker Dimension Icon with ScanAsyst) works in the non-contact mode for the collection of the *height sensor* (morphology) and the *phase* (stiffness) images across the samples. The terms *height sensor* and *phase* for images are specific to Bruker's Nanoscope analysis software. The scan rates are 0.747 Hz, gathering 256 pixels/line and 256 lines/sample to produce scans of 10 $\mu$m $\times$ 10 $\mu$m. The AFM characterizations are done after the drying of the substrate in the oven. Section 1 of the Supporting Information gives details about the scanning procedures.

We use AFM parameters, $R_q$, the root-mean-square of roughness, and $R_{max}$, the distance between highest and the lowest point calculated using a datum line to analyze our results

for the entire slide. Section 1.1 of the Supporting Information provides expressions and details for the calculation of $R_q$ and $R_{max}$ from pixel data. The parameters, $R_q$ and $R_{max}$, in our study reflect the information about the morphology over the entire scan area of 10 $\mu$m $\times$ 10 $\mu$m. For a more detailed analysis, we also carry out cross-section analysis using the *Section Analysis* tool on AFM analysis software. The cross-section analysis is used to acquire information about the fraction of asphaltene on the surface by analyzing pixel-wise information from the scan. The pixel height data is extracted by sketching 36 lines, each of length 3 $\mu$m, across the image. The procedures for carrying out the cross-section analysis using the *Section Analysis* tool are given in Section 1.2 of the Supporting Information. The cross-section analysis also highlights the change in the height distribution of asphaltene structures on the glass slide. The results reported in the entire study are obtained from AFM analysis of a set of eight different experiments carried out under the same conditions. This includes the section analysis, which is used to predict the percentage coverage and the volume analysis.

## 2.5 Contact Angle Measurements

The Kruss DSA-100S records the contact angles at several locations in intervals of five minutes on a single slide. A sessile drop is placed on the glass slide (clean or otherwise asphaltene treated) through a micropipette dispensing a volume of 2 $\mu$L. The drop is allowed to rest for one minute to attain equilibrium shape. The equipped camera captures the live view of the droplet at 200 fps for an image of 1200 $\times$ 800 pixels. The determination of baseline and contact angles are through the assisted software after the image is frozen. Figure S1 in Section 2 of the Supporting Information shows schematic of a droplet placed on a substrate highlighting the contact angles on the left and right of the droplet. The software estimates the contact angles on the left ($\theta_L$) and right ($\theta_R$) by drawing tangents at the drop outline and the baseline intersections. The water contact angle, $\theta_m$ reported in this study, is the average of measured contact angles $\theta_L$ and $\theta_R$ along with their standard deviations from 20

measurements per sample.

# 3 Results and discussion

From the AFM analysis of the untreated glass slide, we report the roughness ($R_q$) of glass slide as 7±1 nm, which reduces to about 0.3 nm after cleaning. The $R_{max}$ value did not exceed 1 nm for the clean glass slide. A much narrower range of phase angle of ±2°, further confirms the cleaning of the slide. A wider range of phase angle in AFM images is obtained in the case of heterogeneity in constituents on the surface.[44,45] The recorded contact angles are also less than 5°, suggesting a highly hydrophilic nature of clean glass slides.[46]

We report a similar surface analysis and contact angle measurement of the substrates for all proceeding experiments involving deposition and asphaltene removal. After 24 hours of aging in the asphaltene dispersion (Figure 1a), the substrates are dipped in pure heptane in three different vials to rinse-out free heptane-asphaltene dispersion from the surface. The tendency of toluene to solubilize asphaltene deposited on the substrates can render the slide ineffective for any further removal studies.[19] Hence, using toluene for substrate rinsing is avoided. Once done with the heptane rinsing process, we test the effect of hydrodynamic forces in the parallel plate channel resulting in the removal of asphaltene from the surface. The drying of the substrates follows for the next 24 hours in the hot air oven at 90°C before the AFM characterizes the substrate for morphological changes on the substrates. The drying of the substrates at 90°C for 24 hours ensures the removal of heptane or any unbounded water from the surface asphaltene. The subsequent sub-sections discuss the results from the deposition and removal experiments of asphaltene from the substrate.

## 3.1 Deposition of Asphaltene

The asphaltenes tend to aggregate, leading to phase separation in a non-polar solvent like *n*-heptane.[47] Upon introducing a silica surface in such a system results in the deposition

of asphaltene aggregates on the surface. The deposition is due to the binding of polar polyaromatic rings and heteroatomic groups with the silica surface wherein van der Waal interactions play major role. The resulting non-uniform deposition on the surface leads to an increase in surface roughness of the substrates.[18,48,49]

The earlier section mentions the method of asphaltene deposition by suspending the glass slides in a heptane-asphaltene dispersion (Figure 1a). The root-mean-square of roughness, $R_q$ for the asphaltene substrates after rinsing with heptane, is found to be 38±8 nm. The results presented here are from experiments repeated eight times. Figure 4 shows representative *height sensor* and *phase* images of a substrate aged in heptane-asphaltene dispersions. The wide variation in the surface roughness in the *height sensor* image suggests the deposition of asphaltene aggregates of different sizes along with regions of no deposition. The wide range of phase angle obtained from AFM, as shown in Figure 4b, supports the argument of heterogeneous deposition at length scales observable by AFM imaging. The lighter contrast corresponds to the higher stiffness (substrate) region, and the darker region represents lower stiffness material corresponding to asphaltene deposition.[50,51] The mean contact angle, $\theta_m = 83.85\pm3^\circ$ , is obtained for the substrates a change in wettability from water-wet to oil-wet, due to the presence of asphaltene on the surface.[52]

## 3.2 Removal of Asphaltene by Shear Forces

Mechanical forces generated by the flow of water in the parallel plate setup are used to remove the deposited asphaltene from the glass slide surface. We hypothesize that when the hydrodynamic forces overcome the adhesion forces binding the asphaltene with asphaltene or asphaltene with the glass surface, detachment is going to occur. The removal of asphaltene from the glass surface is quantified using AFM measurements of the substrate. The AFM measurements are performed at the end of the 20-minute flow cycle that is followed by the drying of the substrates.

The shear rates are exerted over a range from *stagnant* (zero) to $2.37\times10^4$ $s^{-1}$ (Table

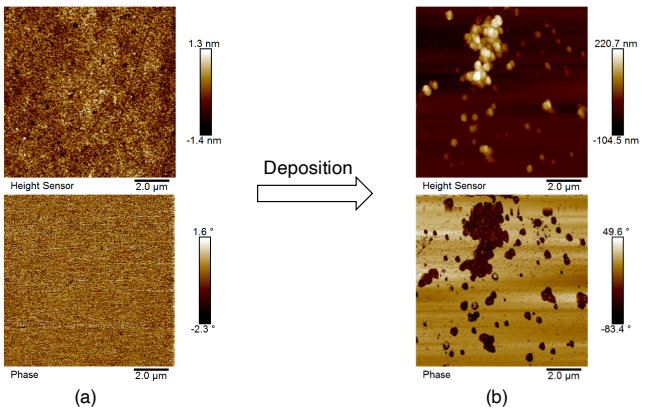


Figure 4: AFM images of a glass slide (a) clean, (b) after aging in heptane-asphaltene suspension and rinsing in pure heptane. The height sensor and phase images are on the top and bottom, respectively. The $R_q$ increases from 0.38 nm (clean) to 39.70 nm after asphaltene deposition. The clean glass slides are homogeneous surfaces, having much lower phase angles and similar contrast. After the deposition the phase angles greatly changed. The light regions correspond to substrate and dark regions represent asphaltene.

1). Figure 5 shows variation in the $R_q$ and $R_{max}$ of substrates as a function of $\dot{\gamma}$. The results shown here are the arithmetic mean of eight different experiments carried out under similar conditions for each data point. In the *stagnant* state, the aged slide is kept inside the channel under no-flow condition. The channel is filled with water by slowly opening the flow control valve, as shown in Figure 3, which is closed afterward when water starts trickling at the other end of the channel. The *stagnant* state accounts for the effect of water on the surface morphology of the substrates in the absence of any shear forces. The *height sensor* and *phase* images of the substrates subjected to shear rates from 0 $s^{-1}$ to $2.37\times10^4$ $s^{-1}$ are shown in Figure 6.

For the case of contact of asphaltene substrate with stagnant water, we observe the increase in roughness from 38 nm (*heptane rinsed*) to 70±6 nm (*stagnant*). Zhang et al.[53] observed a similar increase in roughness with the formation of "pancake-like" domains on mica coated with a thin film of asphaltene contacted with water. The author[53] observed the thickness of deposition to increase from 1 nm to 19 nm with the introduction of asphaltene coated surface in an aqueous media of pH 8.5. The increase in roughness and change in morphology is because of the possible absorption of water molecules and their interaction

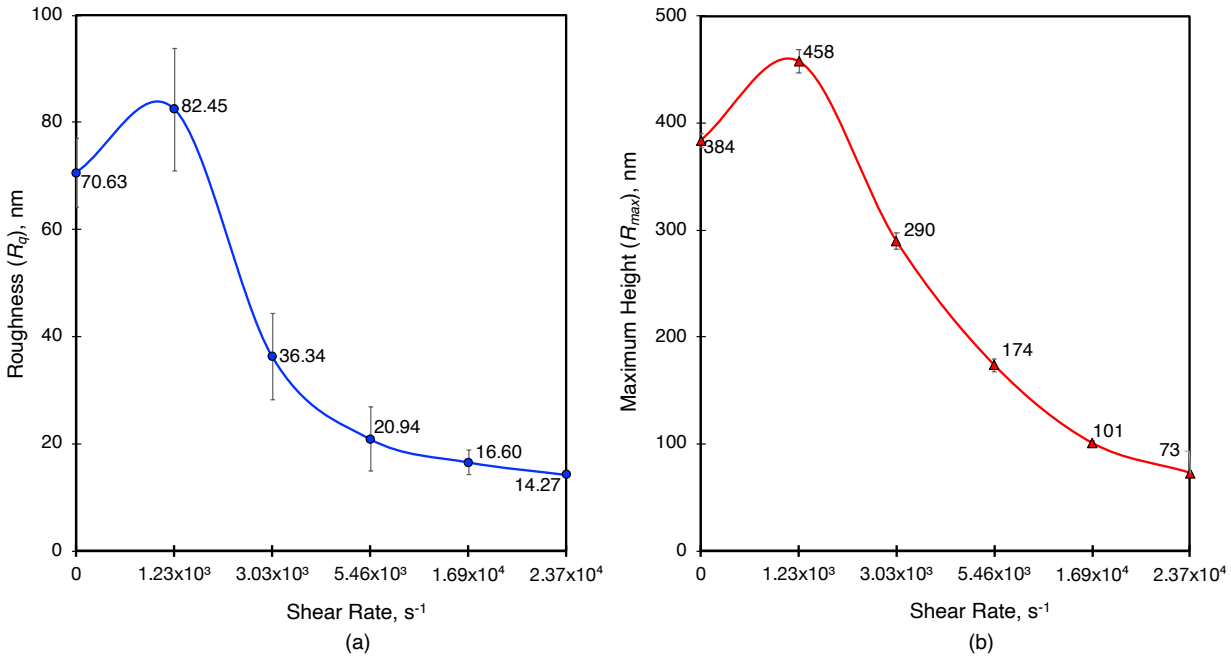


Figure 5: AFM analysis of substrates from the parallel plate channel as a function of $\dot{\gamma}$: (a) $R_q$ (●) and (b) $R_{max}$ (▲). The values mentioned are the mean obtained for eight experiments and the error bars show standard deviations.

with polar groups of asphaltene, which resulted in swelling of aggregates. In this work, while we do not observe any separate "pancake" structure formation, there is a visible increase in the size of the aggregates deposited. The overall volume of asphaltene deposited (shown later) on the surface also increases, suggesting that the increase in roughness of *Stagnant* substrates is due to absorption of water molecules and not because of any mechanical forces. We have also observed the change in the roughness of deposited asphaltene as a function of aqueous media pH under stagnant conditions, which will be reported in more detail in a separate work. The pH-dependent change in roughness suggests electrostatic interactions between asphaltene-asphaltene interface and asphaltene-glass interface to play a role in determining aggregate size.

At the next higher shear rate of $1.23\times10^3$ $s^{-1}$, we observe that the $R_q$ value has further increased to 83±11 nm. The magnitude of shear forces is relatively small at this stage. The growth of aggregates is affected by two possible scenarios. First, the interaction with water molecules with asphaltene causing an increase in the size as observed in the case of the

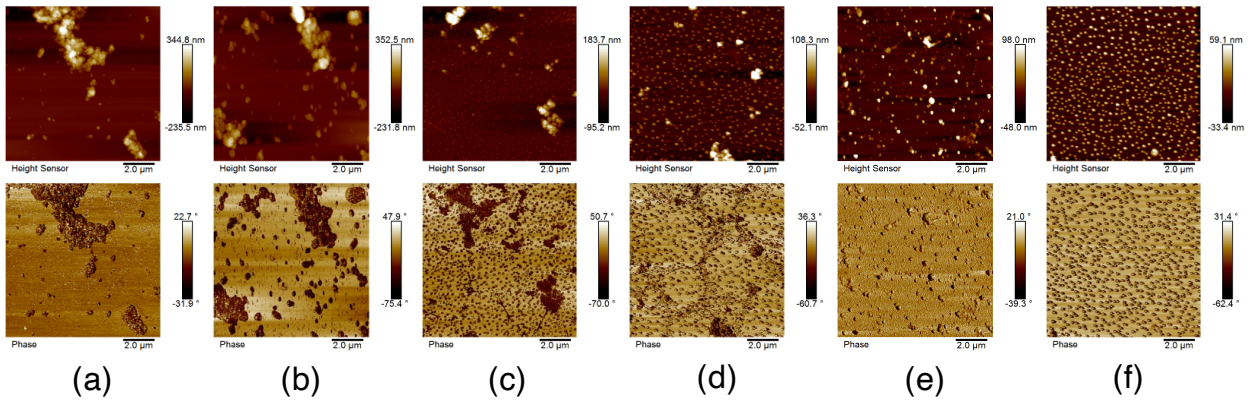


Figure 6: Height sensor (top) and phase images (bottom) of heptane rinsed substrates subjected to various shear rates in the parallel plate channel: (a) Stagnant (zero shear rate), (b) $1.23\times10^3$ $s^{-1}$, (c) $3.03\times10^3$ $s^{-1}$, (d) $5.46\times10^3$ $s^{-1}$, (e) $1.69\times10^4$ $s^{-1}$, and (f) $2.37\times10^4$ $s^{-1}$.

Stagnant state. Secondly, at this stage, the weathering of larger aggregates initiates with loosely bound clusters detaching from these aggregates. The frequency of smaller aggregates to either arrest back to the surface or, in other cases, attach to another aggregate is high due to the lower magnitudes of hydrodynamic forces. The rearrangement of aggregates also increases the relative height of the aggregate ($R_{max}$) as recorded for the substrate at this shear rate. However, the overall volume of the aggregates (shown later) decreases, suggesting that there is a net removal of asphaltene from the substrate. It is to be noted that in our study, we find asphaltene sizes from a few to a few hundred nanometers, and for consistency, we are addressing asphaltene clusters as smaller aggregates.

The roughness declines significantly at a shear rate of $3.03\times10^3$ $s^{-1}$, and the trend continued till $1.69\times10^4$ $s^{-1}$. At this shear rate and beyond, the roughness attained a value of $\approx$ 15 nm that remained similar even at the maximum shear rate of $2.37\times10^4$ $s^{-1}$. The *height sensor* and *phase* images suggest fragmentation of asphaltene aggregates as the shear rates are increased. At the highest shear rate, most of the large aggregates (>100 nm) are removed, as shown by $R_{max}$ in Figure 5. However, the cross-section analysis of the substrate (discussed below) suggests a substantial coverage of the surface with small-sized aggregates. The contact angle analysis further supports the results where the change in contact angle is negligible, even for the highest flow rate (Section 2 of the Supporting Information).

It should be noted here that the redistribution of asphaltene aggregates on the surface could also explain the reduction of surface roughness ($R_q$) from regions of high concentration to low concentration resulting in the flattening of the surface. Here, we use cross-section analysis across the AFM scans to show that the reduction in roughness observed in this work is due to the removal of asphaltene aggregates, instead of aggregates flattening or redistributing on the surface. The cross-section analysis of the *height sensor* image reveals the height of an individual pixel present on an asphaltene structure in the scan. The volume of the asphaltene structure can also be obtained by multiplying the pixel height with the area of a single pixel. The cross-section analysis here accounts for the height distribution of asphaltene structures on the substrates. The analysis is a modified approach taken by Raj et al.[51] for estimation of the size of aggregates of asphaltene on a mica surface. It is worth noting that a single pixel recorded does not correspond to an individual particle on the surface but only a part of the asphaltene particle or aggregate.

Figure 7 shows a model approach to the cross-section analysis of a *stagnant* substrate by sketching three lines of 3 $\mu$m each. The extraction of a datum or the zero line is from a region (green markers), where using *phase* image, it is said to be a region of greater stiffness corresponding to a glass slide. The maximum variation in height between the green markers is less than a nanometer. The phase angle is also within $\pm 1^{\circ}$, which confirms to a region of no deposition. The other two markers, blue and red, are sketched on a location where morphology appears to be divergent due to the presence of asphaltene.

Approximate height distribution of pixels on the surface is obtained by simultaneously sketching 36 lines of 3 $\mu$m each, similar to the ones shown in Figure 7, to account for most of the features on the scan. The normalization of the height distribution of all the pixels with the datum line (zero) assumes that the datum is in a region of no deposition, also supported by the *phase* images. This normalization accounts for estimating the relative amount of material (asphaltene) on the surface. Figure 8 shows the percentage coverage of the surface at four shear rates for various size ranges above 10 nm. The percentage coverage of the

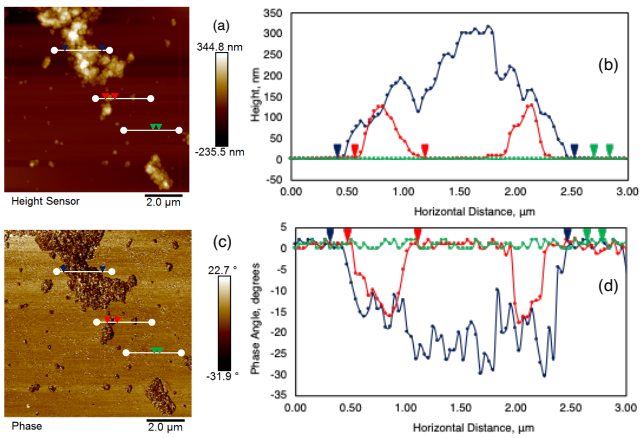


Figure 7: Cross-section analysis of substrates from the parallel plate channel at stagnant (zero) shear rate: (a) and (c) Height sensor and phase image with markers at three different regions to account for morphology and phase angles along the line. (b) and (d) The height and phase angles of pixels along the line sketched. The markers are on the same location as on the left.

surface less than 10 nm, is between 60-70% for all the shear rates, including those not shown in the figure, and thus not mentioned here. In the figure, the four shear rates mentioned highlight the relevant scenarios at zero shear rate, the low shear rate of $1.23\times10^3$ $s^{-1}$, the intermediate shear rate of $5.46\times10^3$ $s^{-1}$, and the highest shear rate of $2.37\times10^4$ $s^{-1}$. The percentage coverage shown in Figure 8 is calculated as (number of pixels in size range)/(total number of pixels) $\times$ 100. There is a total of 2808 pixels extracted from the cross-section analysis on each sample. (See Section 1 of the Supporting Information for more details).

The volume occupied by asphaltene on a pixel is calculated as,

$$V_i = Z_i \frac{10\mu\text{m} \times 10\mu\text{m}}{256 \times 256}$$

where $Z_i$ corresponds to height of the deposited asphaltene on pixel '$i$' and $V_i$ is the volume of asphaltene on the pixel. The total volume ($V_t$) of asphaltene deposited on 2808 pixels of the cross-sectional analysis is calculated as

$$V_t = \sum_{1}^{2808} V_i$$

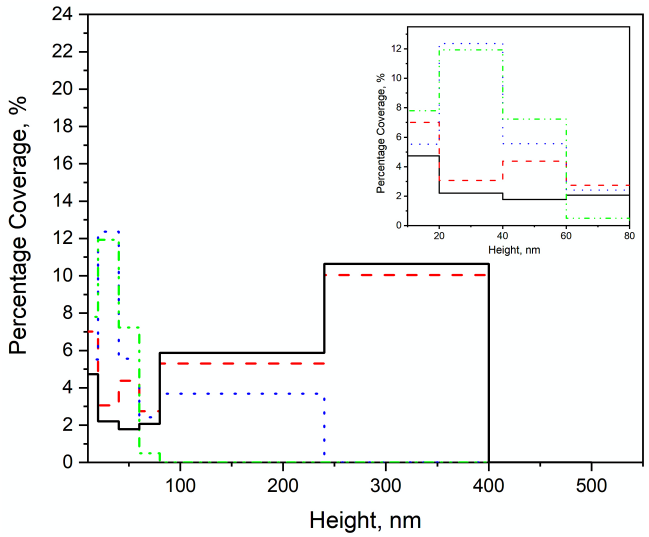


Figure 8: Height distribution of pixels on the substrates in percentage. The shear rates shown in the plot are: Stagnant (—), $1.23\times10^3$ $s^{-1}$ (- -), $5.46\times10^3$ $s^{-1}$ (····), and $2.37\times10^4$ $s^{-1}$ (-·-·). The summation of percentage coverage of individual bars representing various size ranges is an estimation of amount of material (asphaltene) on the surface. The sub-plot is an enlargement of the scale from 0 to 80 nm.

We further normalize the total volume with respect to volume of asphaltene ($V_t|_{stagnant}$) deposited on the substrate at zero shear rate. The total normalized volume at a shear rate is given by, $\bar{V_t} = V_t/V_t|_{stagnant}$.

Figure 8 shows the fraction of the area occupied by the different aggregate sizes of asphaltene on substrates. At low shear rates, there is significant coverage of aggregates of considerable size. As the shear rates increases, the percentage coverage of aggregates greater than 100 nm significantly reduced. However, the count of smaller aggregates increases at higher flow rates suggesting that larger aggregates are not getting completely removed, and part of the aggregate in contact with the silica surface stays behind. At the highest shear rate of $2.37\times10^4$ $s^{-1}$, there is a narrower distribution, size of the largest aggregate is less than 80 nm, and the percentage fraction of small aggregates in the range of 10 nm to 60 nm is much more significant than the zero shear rate case. Figure 9 shows the total normalized volume ($\bar{V_t}$) of asphaltene for various substrates under different shear rates calculated using summing up the volume of asphaltene on each pixel ($\sum V_i$) and normalizing it with the total

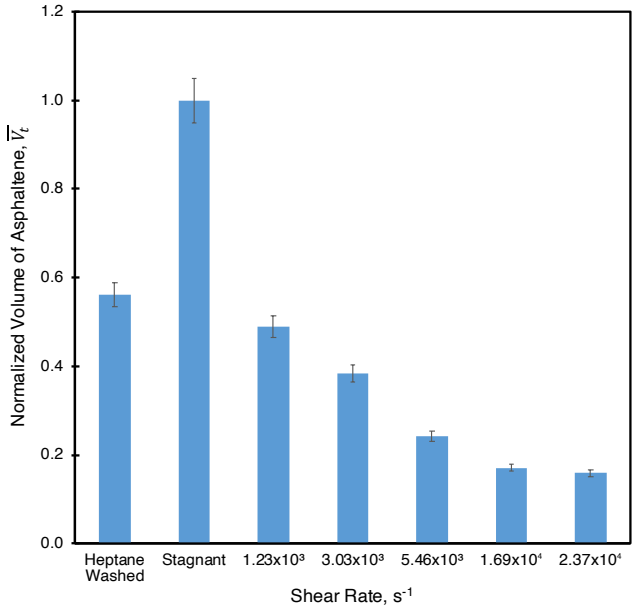


Figure 9: The volume of asphaltene deposited on the heptane washed slide and after cleaning at various shear rates. The volume $\bar{V}_t$ is obtained after normalizing $\sum V_i$ with the total volume of asphaltene on the *stagnant* substrate. $\sum V_i$ is calculated by multiplying the height of 2808 pixels with the area occupied by the pixel, i.e., $(10\mu\text{m} \times 10\mu\text{m})/(256 \times 256)$.

volume of asphaltene on the *stagnant* glass slide. The decrease in the volume of aggregates signifies the removal of asphaltene from the surface. As discussed earlier, the increase in the total volume on transferring the slide from heptane to aqueous media suggests an increase in asphaltene aggregate size due to interactions with the polar solvent. The subsequent reduction in total volume deposited in the cross-sectional analysis corresponds to a lower amount of asphaltene on the substrate at higher flow rates.

Summarising the inferences from the cross-sectional analysis and the normalized volume of asphaltene on the substrate, aggregates are not efficiently remove from the surface at lower shear rates. As the shear rates are increased, large aggregates are weathered due to the hydrodynamic forces. At the highest shear rate ($2.37\times10^4$ $\text{s}^{-1}$), we found aggregates of sizes greater than 80 nm are absent from the surface. The remnants of the large aggregates in the form of smaller ones are still left. The height distribution plot and the volume plot, along with asphaltene roughness results, suggest that the asphaltene has significantly been removed at high shear rates from the surface.

The water contact angles on substrates from the parallel plate channel reported hydrophobicity in all the substrates. The details of these experiments are in Section 2 of the Supporting Information. The asphaltene deposited substrates (after drying) directly observed for water contact angles ($\approx 83^{\circ}$) are similar to those found in the literature for hydrophilic silica coated with asphaltene.[53] Interestingly, we observe an increase in the contact angles ($110^{\circ}$– $125^{\circ}$) on substrates from the parallel plate channel after removal of asphaltene. With lower amount of asphaltene on the surface, one would not expect the contact angle to increase which we observe. The possible explanation for the increase in contact angle for the substrate is again the reorientation of asphaltene on the surface when substrates are left in contact with water for some time (20 minutes in our case). We went a step further to investigate the effect of time on contact angle of a drop when left on the substrate. In this case, the contact angle did not change significantly over first 30 minutes. However, when the drop is left for an hour, the contact angle decreases as slightly. The drying of substrates does not affect the reorientation. As a test sample, substrates without oven drying also showed similar range of contact angles. The hydrophobic chain on the free surface increases the contact angle. This kind of reorientation of amphiphilic molecules to minimize the surface energy and increase in contact angle is also seen in the polymer coated surfaces[54] and hydrogels.[55] The results show no significant variation in contact angles for either of the substrates treated with asphaltene even after the removal experiments. An almost constant contact angle is due to a lack of complete removal of asphaltene from the silica substrate. No correlation could be established between the amount of asphaltene to contact angles.

## 3.3 Nature of Interaction Forces

The detailed AFM analysis shows that large aggregates of asphaltene get removed from the surface at high shear rates. However, the number of small aggregates on the surface increase, suggesting the removal of asphaltene from the asphaltene-asphaltene layers instead of the asphaltene-silica interface. It is also interesting to note that the substrate's surface

coverage by asphaltene patches after the hydrodynamic treatment is homogeneous and has no directional preference with respect to the flow. Once the aggregate is removed, it does not get adsorbed downstream of the flow on the surface. Visser's[27] flow experiments with the removal of carbon black particles also showed similar homogeneous distribution of particles. Here, we estimate the adhesive forces holding the asphaltene aggregates using the hydrodynamic forces applied by the flow.

To estimate the hydrodynamic forces acting on the asphaltene aggregates in the parallel plate channel, we assume the aggregates to be rigid sphere on a flat wall. In such a representation, the asphaltene aggregate of diameter, $d$ adheres to the surface with an effective contact radius ($a_c$), which is related to the aggregate's mechanical properties. The detailed expressions for the calculation of $a_c$ are given in Section 3 of the Supporting Information. In the vicinity of the surface, Reynolds number based on the local velocity and particle diameter is small, and steady-state simple shear flow is assumed.

Various forces acting on a particle adsorbed on a flat surface in steady state shear flow are shown in Figure 10. At low Reynolds number, for a freely suspended particle under an external flow, net force and net torque acting on the particle is zero. However, a net force and a net torque act on a particle when its held stationary in simple shear flow in a non-zero velocity plane. A viscous drag force acting on a stationary spherical particle suspended in a uniform flow of velocity, $U$ is given by $3\pi\mu U d$. For a stationary particle attached to a wall in simple shear flow with center at a distance $d/2$ from the wall, as shown in Figure 10, the modified drag or sliding force on the particle in the direction of the flow is given by,[56]

$$F_D = 1.67(3\pi\mu\dot{\gamma}d^2) \tag{1}$$

At low Reynolds number when a particle is held stationary in a rotating flow field, a torque acts on the particle. The torque due to the rotational component of the simple shear

flow when the particle is held close to the wall is given by,[57,58]

$$M_D = 0.94(2\pi\mu\dot{\gamma}d^3) \tag{2}$$

In simple shear flow a particle also experiences lift force ($F_L$) normal to the direction of flow and away from the wall when one accounts for the effect of inertia, the lift force is given by,[59]

$$F_L = 1.62\left[(\rho\mu)^{1/2}\dot{\gamma}^{3/2}d^3\right] \tag{3}$$

The above three hydrodynamic forces can lead to the removal of the particle by lift, sliding, or rolling. Previously, it has been shown that small particles can detach from a surface via rolling at lower shear rates compared to the shear rates needed for sliding or lifting.[60,61] Our calculations also suggest rolling to be the most feasible mechanism for the removal of the aggregate. Here we compare the torque due to the adhesive force with the torque due to the hydrodynamic forces acting on the sphere at point P, shown in Figure 10. For removal of asphaltene, the hydrodynamic torque should balance torque due to adhesive forces as given by,[60,62]

$$\left[M_D + \left(F_L \cdot a_c + F_D \cdot \frac{d}{2}\right)\right] \geq F_{adh} \cdot a_c \tag{4}$$

In the above equation 4, the three terms on the LHS constitute the total hydrodynamic torque, $M_h$ exerted by the flow on the particle about a point, P. The first term is due to the rotational component of simple shear flow, the second term is due to the lift force, and the third component of torque is due to the sliding force, respectively. The size of the particle, $d$ used in equation 4 is the $R_{max}$ obtained from the AFM analysis (Figure 5). Using the above torque balance we estimate the asphaletene-asphaltene size normalized average adhesive force acting between a spherical aggregate of asphaltene of size, $d$ with an asphaltene layered surface to be, $F_{adh}/(d/2) \approx 1.29$ mN/m. The approximations for the adhesion forces between asphaltene-asphaltene by van der Waals interactions under different conditions are present

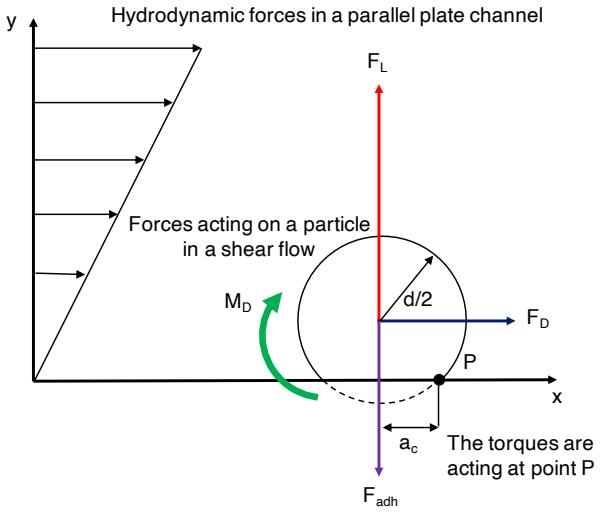


Figure 10: Interaction forces in asphaltene deposition and removal: $F_{adh}$, $F_L$, $F_D$, and $M_D$ are adhesion force, lift force, sliding force, and moment of rotational component, respectively.

in the literature.[20,21,63] Liu et al.[64] estimated the adhesion force between two asphaltene surfaces in aqueous media at pH 8.5 with 1 mM KCl to be around $F_{adh}/(d/2) \approx 5.7$ mN/m. It should be noted here that in this work we carried out experiments at a pH of 7 with DI water. Figure 11 shows the comparison of the moment of adhesion using the results from Liu et al.[64] with the hydrodynamic torques generated by shear flow.

Here we have used the physical properties of water, $\mu = 8.9 \times 10^{-4}$ Pa.s and $\rho = 1.0 \times 10^3$ kg.m$^{-3}$. As evident from Figure 11, the torque due to the hydrodynamic forces applied by the flow is lower as compared to the adhesive forces approximated using values given by Liu et al.[64] The difference increases as the Reynolds number increases and the size of the aggregate ($R_{max}$) adsorbed on the surface decreases. It should also be noted that the moment of sliding acting on the particle and torque due to the rotational component is much larger than the moment of the lift force.

Previous works report that in a turbulent flow, the flow in the viscous layer is not steady and is continually interrupted by turbulent bursts.[28,65] In these studies, empirical models have been developed to explain the particle removal using the turbulent burst mechanism. In summary, we would like to state that more detailed studies, like direct particle visualization

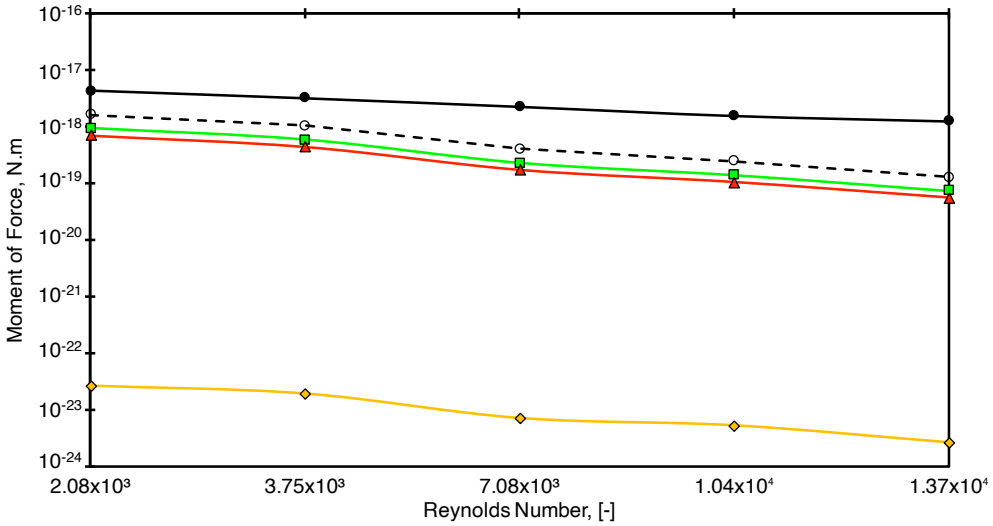


Figure 11: Semi-log plot for moment of forces as a function of Reynolds number. Adhesion torque (●) as approximated by Liu et al.[64] The total hydrodynamic torque, $M_h$ (○) is calculated as a summation of torque due to the lift force (◆), sliding force (■), and rotational component (▲) mentioned in equation 4. The moment of adhesion are slightly higher than the moment of sliding and moment of rotation. The moment of lift is much lower than the adhesion force.

and kinetics of removal, need to be done to ascertain the removal mechanism. Our results show that rolling is the dominant mechanism for removing small asphaltene aggregates from a flat surface, with the possibility of turbulent flow in bulk also playing a role.

# 4 Conclusion

The purpose of the current study was to study the removal of asphaltene using hydrodynamic forces. It was hypothesized that the detachment or removal would occur when the hydrodynamic forces overcome the colloidal forces binding the asphaltene with asphaltene or asphaltene with the glass surface.

The clean glass slides were aged in heptane-asphaltene dispersions under continuous stirring mode for deposition. The removal of asphaltene from the substrates was studied in a fabricated parallel plate channel with water as the shearing fluid. The shear forces on the substrates were tuned by controlling the flow rate inside the channel. The extent of deposition

or removal was expressed in terms of surface morphology changes (roughness and percentage coverage) and surface composition (phase angles) through atomic force microscopy. To conclude the major findings of this study:

- In a non-polar solvent, heptane, the asphaltene aggregates deposit on silica surfaces in the form of patches (aggregates) of uneven thickness. The presence of asphaltene also resulted in increased hydrophobicity of the surface.[3,38,39]

- The size of asphaltene aggregates increase when surfaces were contacted with water. The diffusion of water molecules,[53] and their interaction with hydrophobic alkyl chains results in the reorientation of asphaltene aggregates,[20] causing an increase in the size of aggregates.

- When hydrodynamic forces were increased, the removal initiates with weathering of large aggregates into smaller ones on the surface (Figure 8). The removal occurs from asphaltene layers where the efficiency of removal was found to have increased as a function of increasing shear rates. Aggregate distribution on the surface was observed to be heterogeneous, suggesting no migration of aggregates on the surface due to the flow.

- Balancing the hydrodynamic torque with the adhesive torque, the asphaltene-asphaltene adhesive forces were estimated to be $F_{adh}/(d/2) = 1.29$ mN/m for DI water with pH 7 media. The asphaltene-asphaltene adhesive force measured using the AFM are reported to be $F_{adh}/(d/2) = 5.7$ mN/m[64] for pH 8.2 and 1 mM KCl solution.

- The removal of asphaltene was possibly due to the rolling of aggregates on the surface.[60,61] The much smaller aggregates were sustained on the surface due to limitations of offered shear rates.

- The contact angle measurements also suggest negligible removal of asphaltene in contact with silica as substrates showed partial wettability[52] with almost same contact

angle for all flow rates.

The scope of further studies can be direct particle visualizations and kinetics of removal to ascertain removal mechanism.[28,65] The authors have also investigated the effect of aqueous media pH and ionic surfactants to compare the relative efficiency of removal and will be reported in a separate communication. The findings of the current study provided qualitative information about asphaltene aggregate sizes on the surface and their interaction with the substrate.

# Author Information

**Corresponding Author**

Email: vs225@chemical.iitd.ac.in (Vikram Singh)

# Author Contributions

Vikram Singh and Jyoti Phirani conceptualized and designed the array for work. Anil Yadav has modeled the parallel plate channel used in this study. Syed Haider Abbas Rizvi and Anil Yadav jointly performed the necessary experiments. Syed Haider Abbas Rizvi did the AFM measurements, analysis, and data interpretations. Vikram Singh and Jyoti Phirani provided the critical revision of the article. Syed Haider Abbas Rizvi, Anil Yadav, Jyoti Phirani, and Vikram Singh gave the final approval for the version to be published.

# Funding Sources

Shell Technology Centre Bangalore, India, financially supported the work.

## Notes

The authors declare no competing financial interest.

## Acknowledgement

The authors gratefully acknowledge Dr. Sudip K. Pattanayek (Professor, Department of Chemical Engineering, IIT Delhi) and Dr. J. P. Singh (Professor, Department of Physics, IIT Delhi) for their support in characterization and analysis. The Nanoscale Research Facility to conduct AFM imaging of the samples, Macromolecules and Interfaces Laboratory for contact angle measurements at Indian Institute of Technology, Delhi. The authors are thankful to Shalini Shikha, Vinod Kumar, and Alisha Agarwal for their assistance during experiments.

## Supporting Information Available

Supporting Information A to C provides supplementary data for this communication. Supporting Information A briefs about atomic force microscopy and the parameters for analysis of images. Supporting Information B contains details about the measurement of contact angles of water on substrates. Supporting Information C deals with correlations for the estimation of effective contact radius of adhesion with definitions for Hamaker constant for the current system. These supplementary data files are available separately and can be found here: Supporting Information for the article

## References

(1) McLean, J. D.; Kilpatrick, P. K. Comparison of precipitation and extrography in the fractionation of crude oil residua. *Energy and Fuels* **1997**, *11*, 570–585.

(2) Yudin, I. K.; Nikolaenko, G. L.; Gorodetskii, E. E.; Markhashov, E. L.; Frot, D.;

Briolant, Y.; Agayan, V. A.; Anisimov, M. A. Universal behavior of asphaltene aggregation in hydrocarbon solutions. *Petroleum Science and Technology* **1998**, *16*, 395–414.

(3) Buckley, J. S. Wetting alteration of solid surfaces by crude oils and their asphaltenes. *Revue de l'Institute Francais du Petrole* **1998**, *53*, 303–312.

(4) Andersen, S. I.; Christensen, S. D. Critical micelle concentration of asphaltenes As measured by calorimetry. *Energy and Fuels* **2000**, *14*, 38–42.

(5) Mitchell, D. L.; Speight, J. G. The solubility of asphaltenes in hydrocarbon solvents. *Fuel* **1973**, *52*, 149–152.

(6) Miadonye, A.; Evans, L. The solubility of asphaltenes in different hydrocarbon liquids. *Petroleum Science and Technology* **2010**, *28*, 1407–1414.

(7) Yen, T. F.; Erdman, J. G.; Pollack, S. S. Investigation of the Structure of Petroleum Asphaltenes by X-Ray Diffraction. *Analytical Chemistry* **1961**, *33*, 1587–1594.

(8) Pfeiffer, J. P.; Saal, R. N. J. Asphaltic bitumen as colloid system. *Journal of Physical Chemistry* **1940**, *44*, 139–149.

(9) Thawer, R.; Nicoll, D. C.; Dick, G. Asphaltene deposition in production facilities. *SPE Production Engineering* **1990**, *5*, 475–480.

(10) Chrisman, E.; Lima, V.; Menechini, P. *Crude Oil Emulsions- Composition Stability and Characterization*; 2012.

(11) Tavakkoli, M.; Panuganti, S. R.; Vargas, F. M.; Taghikhani, V.; Pishvaie, M. R.; Chapman, W. G. Asphaltene deposition in different depositing environments: Part 1. model oil. *Energy and Fuels* **2014**, *28*, 1617–1628.

(12) Hu, X.; Yutkin, M. P.; Hassan, S.; Wu, J.; Prausnitz, J. M.; Radke, C. J. Asphaltene Adsorption from Toluene onto Silica through Thin Water Layers. *Langmuir* **2019**, *35*, 428–434.

(13) Zekri, A. Y.; Shedid, S. A.; Alkashef, H. User of laser technology for the treatment of asphaltene deposition in carbonate formations. *Petroleum Science and Technology* **2003**, *21*, 1409–1426.

(14) Sanada, A.; Miyagawa, Y. A case study of a successful chemical treatment to mitigate asphaltene precipitation and deposition in light crude oil field. *Proceedings - SPE Asia Pacific Oil and Gas Conference and Exhibition 2006: Thriving on Volatility* **2006**, *2*, 654–661.

(15) Kumar, K.; Dao, E. K.; Mohanty, K. K. Atomic Force Microscopy Study of Wettability Alteration by Surfactants. *SPE Journal* **2008**, *13*, 137–145.

(16) Murgich, J. Intermolecular forces in aggregates of asphaltenes and resins. *Petroleum Science and Technology* **2002**, *20*, 983–997.

(17) Adams, J. J. Asphaltene adsorption, a literature review. *Energy and Fuels* **2014**, *28*, 2831–2856.

(18) Natarajan, A.; Kuznicki, N.; Harbottle, D.; Masliyah, J.; Zeng, H.; Xu, Z. Understanding mechanisms of asphaltene adsorption from organic solvent on mica. *Langmuir* **2014**, *30*, 9370–9377.

(19) Wang, S.; Liu, J.; Zhang, L.; Xu, Z.; Masliyah, J. Colloidal interactions between asphaltene surfaces in toluene. *Energy and Fuels* **2009**, *23*, 862–869.

(20) Abraham, T.; Christendat, D.; Karan, K.; Xu, Z.; Masliyah, J. Asphaltene - Silica interactions in aqueous solutions: Direct force measurements combined with electrokinetic studies. *Industrial and Engineering Chemistry Research* **2002**, *41*, 2170–2177.

(21) Labrador, H.; Fernández, Y.; Tovar, J.; Muñoz, R.; Pereira, J. C. Ellipsometry study of the adsorption of asphaltene films on a glass surface. *Energy and Fuels* **2007**, *21*, 1226–1230.

(22) Soorghali, F.; Zolghadr, A.; Ayatollahi, S. Effects of Native and Non-Native Resins on Asphaltene Deposition and the Change of Surface Topography at Different Pressures: An Experimental Investigation. *Energy and Fuels* **2015**, *29*, 5487–5494.

(23) Shkalikov, N. V.; Vasil'ev, S. G.; Skirda, V. D. Peculiarities of asphaltene precipitation in n-alkane-oil systems. *Colloid Journal* **2010**, *72*, 133–140.

(24) Hashmi, S. M.; Loewenberg, M.; Firoozabadi, A. Colloidal asphaltene deposition in laminar pipe flow: Flow rate and parametric effects. *Physics of Fluids* **2015**, *27*.

(25) Al Sultan, A.; Zirrahi, M.; Hassanzadeh, H.; Abedi, J. Effect of the Surfactant on Asphaltene Deposition on Stainless-Steel and Glass Surfaces. *Energy and Fuels* **2018**, *32*, 5635–5642.

(26) Zhuang, Y.; Goharzadeh, A.; Lin, Y. J.; Yap, Y. F.; Chai, J. C.; Mathew, N.; Vargas, F.; Biswal, S. L. Experimental study of asphaltene deposition in transparent microchannels using the light absorption method. *Journal of Dispersion Science and Technology* **2018**, *39*, 744–753.

(27) Visser, J. Measurement of the force of adhesion between submicron carbon-black particles and a cellulose film in aqueous solution. *Journal of Colloid And Interface Science* **1970**, *34*, 26–31.

(28) Cleaver, J. W.; Yates, B. Mechanism of detachment of colloidal particles from a flat substrate in a turbulent flow. *Journal of Colloid And Interface Science* **1973**, *44*, 464–474.

(29) Ranade, M. B. Adhesion and removal of fine particles on surfaces. *Aerosol Science and Technology* **1987**, *7*, 161–176.

(30) Zoeteweij, M. L.; Van Der Donck, J. C. J.; Versluis, R. Particle removal in linear shear

flow: Model prediction and experimental validation. *Journal of Adhesion Science and Technology* **2009**, *23*, 899–911.

(31) Burdick, G. M.; Berman, N. S.; Beaudoin, S. P. Describing hydrodynamic particle removal from surfaces using the particle Reynolds number. *Journal of Nanoparticle Research* **2001**, *3*, 455–467.

(32) Niida, T.; Kousaka, Y.; Furukawa, T. Removal of Adhering Particles of Polystyrene Latex and iron oxide on a wall by shear flow in water. *Particle & Particle Systems Characterization* **1989**, *6*, 69–73.

(33) Hashmi, S. M.; Firoozabadi, A. Effective removal of asphaltene deposition in metal-capillary tubes. *SPE Journal* **2016**, *21*, 1747–1754.

(34) Abarham, M.; Hoard, J.; Assanis, D.; Styles, D.; Curtis, E. W.; Ramesh, N. Review of soot deposition and removal mechanisms in EGR coolers. *SAE Technical Papers* **2010**, 690–704.

(35) Young, R. M.; Hargather, M. J.; Settles, G. S. Shear stress and particle removal measurements of a round turbulent air jet impinging normally upon a planar wall. *Journal of Aerosol Science* **2013**, *62*, 15–25.

(36) Efe-Sanden, G.; Gallant, N.; Alcantar, N.; Toomey, R. Adhesion and particle removal from surface-tethered poly(n-isopropylacrylamide) coatings using hydrodynamic shear Forces. *Langmuir* **2019**, *35*, 15751–15758.

(37) Meinders, J. M.; Busscher, H. J. Adsorption and desorption of colloidal particles on glass in a parallel plate flow chamber-Influence of ionic strength and shear rate. *Colloid & Polymer Science* **1994**, *272*, 478–486.

(38) Gloton, M. P.; Turmine, M.; Mayaffre, A.; Letellier, P.; Toulhoat, H. Study of asphaltenes adsorption on mineral surfaces by contact angle measurements: kinetics of

wettability changes. *Physical Chemistry of Colloids and Interfaces in Oil Production* **1992**, 89–96.

(39) Ratnakar, R. R.; Mantilla, C. A.; Dindoruk, B. Impact of Asphaltenes on Contact-Angle Variations and Surface Topography and Composition. *SPE Journal* **2020**, *Preprint*, 14.

(40) Wang, J.; Buckley, J. Standard Procedure for Separating Asphaltenes from Crude Oils. *PRRC Biannual Newsletter* **2002**,

(41) Gaud, F. Die gewichtsanalytische Bestimmung des Zuckers. *Zeitschrift für Analytische Chemie* **1895**, *34*, 251–252.

(42) Li, Z.; Yin, J.; Zhu, D.; Datta-Gupta, A. Using downhole temperature measurement to assist reservoir characterization and optimization. *Journal of Petroleum Science and Engineering* **2011**, *78*, 454–463.

(43) Alves, I. N.; Alhanati, F. J. S.; Shoham, O. A Unified Model for Predicting Flowing Temperature Distribution in Wellbores and Pipelines. *SPE Production Engineering* **1992**, *7*, 363–367.

(44) Scott, W. W.; Bhushan, B. Use of phase imaging in atomic force microscopy for measurement of viscoelastic contrast in polymer nanocomposites and molecularly thick lubricant films. *Ultramicroscopy* **2003**, *97*, 151–169.

(45) Cheng, S.; Bryant, R.; Doerr, S. H.; Rhodri Williams, P.; Wright, C. J. Application of atomic force microscopy to the study of natural and model soil particles. *Journal of Microscopy* **2008**, *231*, 384–394.

(46) Sumner, A. L.; Menke, E. J.; Dubowski, Y.; Newberg, J. T.; Penner, R. M.; Hemminger, J. C.; Wingen, L. M.; Brauers, T.; Finlayson-Pitts, B. J. The nature of water on surfaces of laboratory systems and implications for heterogeneous chemistry in the troposphere. *Physical Chemistry Chemical Physics* **2004**, 604–613.

(47) Wang, S.; Liu, J.; Zhang, L.; Masliyah, J.; Xu, Z. Interaction forces between asphaltene surfaces in organic solvents. *Langmuir* **2010**, *26*, 183–190.

(48) Andrews, A. B.; McClelland, A.; Korkeila, O.; Demidov, A.; Krummel, A.; Mullins, O. C.; Chen, Z. Molecular orientation of asphaltenes and PAH model compounds in langmuir-blodgett films using sum frequency generation spectroscopy. *Langmuir* **2011**, *27*, 6049–6058.

(49) Vuillaume, K.; Giasson, S. Interactions between mica surfaces across crude oil and asphaltene solutions. *Journal of Physical Chemistry C* **2009**, *113*, 3660–3665.

(50) Balestrin, L. B. D. S.; Cardoso, M. B.; Loh, W. Using Atomic Force Microscopy To Detect Asphaltene Colloidal Particles in Crude Oils. *Energy and Fuels* **2017**, *31*, 3738–3746.

(51) Raj, G.; Lesimple, A.; Whelan, J.; Naumov, P. Direct Observation of Asphaltene Nanoparticles on Model Mineral Substrates. *Langmuir* **2017**, *33*, 6248–6257.

(52) Acevedo, S.; Ranaudo, M. A.; García, C.; Castillo, J.; Fernández, A. Adsorption of asphaltenes at the toluene-silica interface: A kinetic study. *Energy and Fuels* **2003**, *17*, 257–261.

(53) Zhang, L.; Xie, L.; Shi, C.; Huang, J.; Liu, Q.; Zeng, H. Mechanistic Understanding of Asphaltene Surface Interactions in Aqueous Media. *Energy and Fuels* **2017**, *31*, 3348–3357.

(54) Yasuda, T.; Okuno, T.; Yasuda, H. Contact angle of water on polymer surfaces. *Langmuir* **1994**, *10*, 2435–2439.

(55) Holly, F. J.; Refojo, M. F. Wettability of hydrogels I. Poly (2-hydroxyethyl methacrylate). *Journal of biomedical materials research* **1975**, *9*, 315–326.

(56) Goldman, A. J.; Cox, R. G.; Brenner, H. Slow viscous motion of a sphere parallel to a plane wall-II Couette flow. *Chemical Engineering Science* **1967**, *22*, 653–660.

(57) O'Neill, M. E. A sphere in contact with a plane wall in a slow linear shear flow. *Chemical Engineering Science* **1968**, *23*, 1293–1298.

(58) Soltani, M.; Ahmadi, G. On particle adhesion and removal mechanisms in turbulent flows. *Journal of Adhesion Science and Technology* **1994**, *8*, 763–785.

(59) Saffman, P. G. The lift on a small sphere in a slow shear flow. *Journal of Fluid Mechanics* **1965**, *22*, 385–400.

(60) Soltani, M.; Ahmadi, G. Detachment of rough particles with electrostatic attraction from surfaces in turbulent flows. *Journal of Adhesion Science and Technology* **1999**, *13*, 325–355.

(61) Harris, A. R.; Davidson, C. I. Particle Resuspension in Turbulent Flow: A Stochastic Model for Individual Soil Grains. *Aerosol Science and Technology* **2008**, *42*, 613–628.

(62) Thennadil, S. N.; Garcia-Rubio, L. H. Approximations for calculating van der Waals interaction energy between spherical particles - A comparison. *Journal of Colloid and Interface Science* **2001**, *243*, 136–142.

(63) Buch, L.; Groenzin, H.; Buenrostro-Gonzalez, E.; Andersen, S. I.; Lira-Galeana, C.; Mullins, O. C. Molecular size of asphaltene fractions obtained from residuum hydrotreatment. *Fuel* **2003**, *82*, 1075–1084.

(64) Liu, J.; Zhang, L.; Xu, Z.; Masliyah, J. Colloidal interactions between asphaltene surfaces in aqueous solutions. *Langmuir* **2006**, *22*, 1485–1492.

(65) Rashidi, M.; Hetsroni, G.; Banerjee, S. Particle-turbulence interaction in a boundary layer. *International Journal of Multiphase Flow* **1990**, *16*, 935–949.

# Graphical TOC Entry